

# Real-space coherent manipulation of electrons in a single tunnel junction by single-cycle terahertz electric fields

Katsumasa Yoshioka<sup>1</sup>, Ikufumi Katayama<sup>1\*</sup>, Yasuo Minami<sup>1</sup>, Masahiro Kitajima<sup>1,2</sup>, Shoji Yoshida<sup>3</sup>, Hidemi Shigekawa<sup>3\*</sup> and Jun Takeda<sup>1\*</sup>

**The ultrafast coherent manipulation of electrons using waveform-controlled laser pulses<sup>1–9</sup> is a key issue in the development of modern electronics<sup>10,11</sup>. Developing such an approach for a tunnel junction will provide a new platform for governing ultrafast currents on an even smaller scale, which will be indispensable for the advancement of next-generation quantum nanocircuits<sup>12–15</sup> and plasmonic devices<sup>16–18</sup>. Here, we demonstrate that carrier-envelope-phase-controlled single-cycle terahertz electric fields can coherently drive electron tunnelling either from a nanotip to a sample or vice versa. Spatially confined electric fields of more than 10 V nm<sup>−1</sup> strongly modulate the potential barrier at a nanogap in a scanning tunnelling microscope (STM) on the subpicosecond timescale and can steer a large number of electrons in an extremely nonlinear regime, which is not possible using a conventional STM. Our results are expected to pave the way for the future development of nanoscale science and technologies.**

The latest advances in laser technology have made it possible to control the carrier-envelope phase (CEP) of ultrashort laser pulses with high accuracy. Using few-cycle CEP-controlled near-infrared laser pulses, several studies have demonstrated the ultrafast coherent control of electrons in a wide range of systems<sup>1–9</sup>. In these studies, metallic nanostructures, so-called metal nanotips, were used to produce highly localized near-fields by concentrating laser pulses into dimensions far below the diffraction limit of the incident light. Using a spatiotemporally tunable near-field of up to  $\sim$ 10 V nm<sup>−1</sup>, ultrafast electron bursts from a nanotip have been realized<sup>7–9</sup>. These sophisticated electron manipulations will open fascinating avenues for overcoming the bandwidth limitation of signal processing in modern information technology<sup>10,11</sup>.

A larger field enhancement is expected to occur at a tunnel junction<sup>12,14,18,19</sup>. The resulting strong nonlinearity will be useful for the manipulation of electrons at the atomic scale, which is highly desirable for the advancement of next-generation integrated nanocircuits<sup>12–15</sup> and plasmonic devices<sup>16–18</sup>. However, strong near-infrared laser pulses focused on a tunnel junction induce thermal expansion<sup>20</sup>, leading to permanent damage of the junction. Therefore, precise control of the motion of electrons at the atomic scale is still a challenging task. Recently, single-cycle electric field transients with high intensity have been generated in the terahertz (THz) spectral range (0.1–10 THz)<sup>21,22</sup>. In contrast to few-cycle near-infrared laser pulses, single-cycle THz electric fields with a bandwidth over an octave may be useful for accurately steering electrons, and may drive electron tunnelling without heating systems because of their low energy. Indeed, THz-field-induced nonlinear

electron tunnelling has been observed in percolated gold nanostructures<sup>23</sup> and metal–graphene–metal hybrid structures<sup>18</sup> without any thermal effects. Terahertz scanning tunnelling microscopy (THz-STM)<sup>19</sup>, which was developed after optical pump–probe STM<sup>24,25</sup>, may allow ultrafast dynamics to be probed with fewer thermal expansion problems.

Here, we demonstrate real-space coherent manipulation of the motion of electrons in a single tunnel junction by utilizing CEP-controlled single-cycle THz electric fields via the Gouy phase shift<sup>26</sup>. Unlike the imaging of surfaces at the atomic scale using conventional STM, our THz-STM with the tunnel junction presented here acts as an ultrafast rectifying diode or a THz field-effect transistor<sup>7,27</sup>; the electron current is switched on and off via the CEP-controlled single-cycle THz electric fields. The basic concept of our experimental set-up is illustrated in Fig. 1a–c. Intense single-cycle THz electric field transients were generated by optical rectification of femtosecond laser pulses in a LiNbO<sub>3</sub> prism using a tilted-pulse-front configuration<sup>21</sup>. The generated THz pulses were guided into one of two optical paths: one was used for characterizing the THz waveforms by electro-optic sampling (EOS), while the other was used to deliver the THz pulses to a single tunnel junction. The THz pulses were focused onto the apex of a Pt/Ir nanotip. We used highly oriented pyrolytic graphite (HOPG) as the sample because of its atomically flat surface. All measurements were performed under ambient laboratory conditions. By placing either a pair of spherical or cylindrical lenses in the beam path (Fig. 1b), the CEP of the incident THz pulses ( $\phi_{\text{CEP}} = 0$ ) was shifted by  $\phi_{\text{CEP}} = \pi$  or  $\phi_{\text{CEP}} = \pi/2$ , respectively, via the Gouy phase shift. As schematically shown in Fig. 1c, the CEP-controlled single-cycle THz electric field modifies the potential barrier between the nanotip and the sample, leading to the unidirectional coherent motion of electrons. By irradiating the junction with THz pulses with  $\phi_{\text{CEP}} = 0$  (Fig. 1d), a series of tunnel currents were synchronously generated with the same repetition rate as the laser system (1 kHz), as shown in Fig. 1e. Note that the time-integrated value of each current pulse represents the number of rectified electrons driven by a single THz pulse through the junction (see Supplementary Section I).

The CEP dependence of the tunnel current was measured with different CEPs of  $\phi_{\text{CEP}} = 0$ ,  $\pi/2$  and  $\pi$ , while sweeping the d.c. bias from 300 mV to  $-300$  mV (Fig. 2a,b). The most remarkable feature in Fig. 2b is a series of THz-induced pulse trains, which is a fingerprint of the ultrafast current bursts in the tunnel junction. In the case of  $\phi_{\text{CEP}} = 0$ , the pulse train takes a positive value, which corresponds to an electron tunnelling from the nanotip to the sample. The intensity of the pulse train increases with increasing

<sup>1</sup>Department of Physics, Graduate School of Engineering, Yokohama National University, Yokohama 240-8501, Japan. <sup>2</sup>LxRay Company Limited, Nishinomiya 663-8172, Japan. <sup>3</sup>Faculty of Pure and Applied Sciences, University of Tsukuba, Tsukuba 305-8571, Japan.

\*e-mail: katayama@ynu.ac.jp; hidemi@ims.tsukuba.ac.jp; jun@ynu.ac.jp

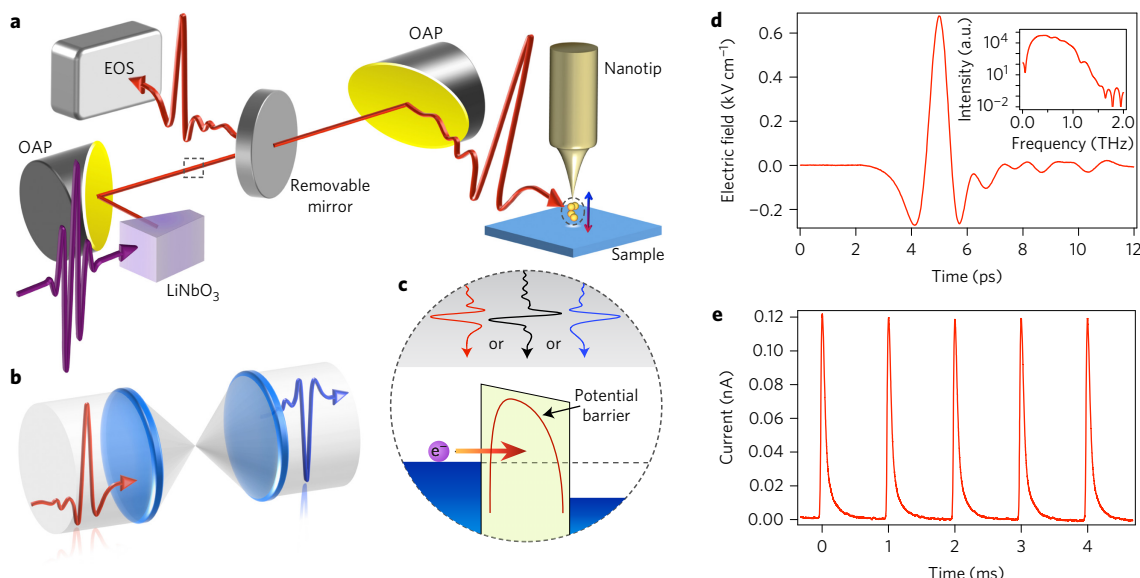


**Figure 1 | Experimental set-up of the THz-STM.** **a**, Schematic of the experimental set-up. CEP-controlled single-cycle THz electric fields are focused onto the apex of a Pt/Ir nanotip at an incident angle of 75°. OAP, off-axis parabolic mirror; EOS, electro-optic sampling. **b**, Schematic illustration of  $\pi$  phase-shift of a THz electric field via the Gouy phase shift using a pair of spherical lenses (dashed square in **a**). A pair of cylindrical lenses is used when a  $\pi/2$  phase-shift is required. **c**, Schematic illustration of an electron ( $e^-$ ) tunnelling between a nanotip and a sample under the influence of a static electric field (dashed circle in **a**). The motion of electrons is coherently controlled by THz electric fields with different CEPs. **d**, Temporal profile of a single-cycle THz electric field ( $\phi_{CEP} = 0$ ) measured using EOS. The inset shows the corresponding THz frequency spectrum. **e**, Pulse train generated by the THz electric field ( $\phi_{CEP} = 0$ ) without any d.c. bias. The feedback loop remained off during the measurement (setpoint: bias voltage  $V_s = 1$  V; tunnel current  $I_s = 1$  nA). The decay profile of each current pulse comes from the bandwidth of the amplifier used in the STM circuits.

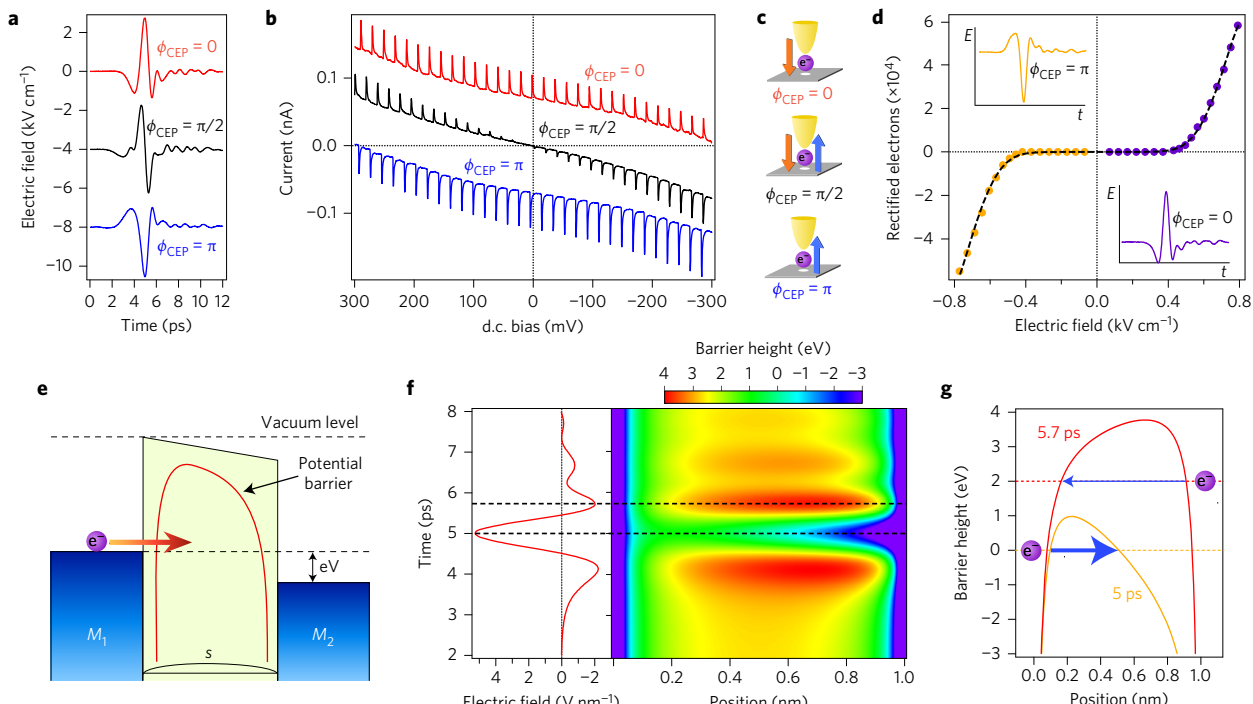


**Figure 2 | Effect of CEP on the motion of tunnelling electrons.** **a**, Temporal profiles of single-cycle THz electric fields with different CEPs ( $\phi_{CEP} = 0, \pi/2$  and  $\pi$ ). **b**, CEP dependence of tunnel current as a function of d.c. bias ( $V_s = 1$  V,  $I_s = 0.5$  nA). The spectra with  $\phi_{CEP} = 0$  and  $\pi$  are offset by  $\pm 0.07$  nA for clarity. **c**, Schematic illustration of the motion of electrons driven by THz electric fields with different CEPs. The orange and blue arrows show the tunnelling direction. **d**, Number of rectified electrons induced by a single THz pulse without d.c. bias as a function of the peak electric field ( $V_s = 1$  V,  $I_s = 1$  nA). The dashed curve shows the best fit obtained by the Simmons model. **e**, Potential barrier between nanotip ( $M_1$ ) and sample ( $M_2$ ) under a bias voltage  $V$ , where  $s$  is the width of the gap between the tip and the sample. **f**, Time dependence of potential barrier under an enhanced THz electric field. **g**, Potential barriers at  $t = 5$  and  $t = 5.7$  ps, which are indicated by the dashed lines in **f**. The electron undergoes tunnelling in the smaller potential barrier at  $t = 5$  ps rather than that at  $t = 5.7$  ps as shown by the thicker and thinner arrows, respectively. The thicker arrow indicates the higher probability of tunnelling.

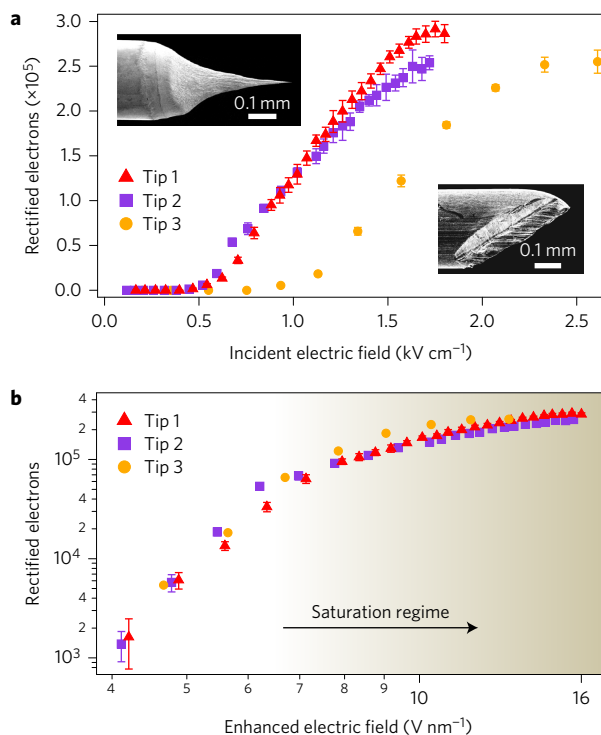


**Figure 3 | Current saturation under strong electric fields.** **a**, Number of rectified electrons without d.c. bias as a function of incident electric field ( $\phi_{CEP} = 0$ ) for different tips ( $V_s = 1$  V,  $I_s = 1$  nA). Tips 1 and 2 (sharp) were fabricated by electrochemical etching whereas tip 3 (blunt) was formed by mechanical cutting. Insets: scanning electron microscopy images of the sharp (top) and blunt (bottom) tips. **b**, Log-scale plot of number of rectified electrons as a function of the enhanced electric field at the tunnel junction. The enhancement factor of tip 3 is  $50,000 \pm 200$ , which is two times smaller than that of the sharp nanotips. Error bars correspond to 95% confidence intervals.

d.c. bias. In the case of  $\phi_{CEP} = \pi$ , on the other hand, the tunnel current shows the opposite behaviour; the pulse train with a negative value indicates an electron tunnelling from the sample to the nanotip. In the case of  $\phi_{CEP} = \pi/2$ , the direction of electron tunnelling strongly depends on the d.c. bias; electrons undergo tunnelling from the nanotip to the sample under a positive d.c. bias and in the opposite direction under a negative d.c. bias. The current pulse disappears as the d.c. bias approaches 0 (see Supplementary Section II). As schematically summarized in Fig. 2c, the coherent motion of electrons at the junction is controlled by the CEP-locked THz pulses with a given d.c. bias.

Figure 2d shows the number of rectified electrons induced by a single THz pulse as a function of the peak electric field with different CEPs ( $\phi_{CEP} = 0$  and  $\phi_{CEP} = \pi$ ). The nonlinear increase in the number of rectified electrons with the THz electric field was numerically evaluated on the basis of the Simmons model<sup>28</sup> assuming a potential barrier between the nanotip ( $M_1$ ) and the sample ( $M_2$ ) under a bias voltage  $V$ , as illustrated in Fig. 2e. As shown by the dashed line in Fig. 2d, the experimental data are accurately reproduced with the adjustable parameters of an effective workfunction of  $3.8 \pm 0.1$  eV, a gap width of  $1.00 \pm 0.01$  nm and an enhancement factor of  $100,000 \pm 10,000$ . These values were also confirmed by current-distance ( $I-Z$ ) and d.c. current-voltage ( $I-V$ ) experiments (see Supplementary Section III). The large field enhancement originates from the extremely tight focusing of the THz electric field onto the single junction with a 1 nm gap between the sample and the nanotip induced by the broadband antenna effect of the nanotip and/or the plasmonic effect at the tunnel junction<sup>8,14</sup>. The

time-dependent modulation of the potential barrier was also calculated using the Simmons model. As shown in Fig. 2f,g, the potential barrier is coherently distorted by the enhanced THz electric field at the junction. For example, the barrier height is reduced to 0.98 eV whereas the barrier width decreases to 0.41 nm at the field strength of  $+5.3$  V nm<sup>-1</sup>. In contrast, a field strength of  $-2.0$  V nm<sup>-1</sup> causes the barrier to shrink less, with the height and width reduced to 1.78 eV and 0.75 nm, respectively. This potential asymmetry driven by the CEP-locked single-cycle THz electric field leads to unidirectional electron tunnelling through the junction on the subpicosecond timescale.

By further increasing the THz electric field, we can implement a new regime for electron tunnelling that is inaccessible by conventional STM. The results are shown in Fig. 3a for three different tips: two sharp nanotips (tips 1, 2) and one blunt tip (tip 3) as shown in the inset. The curves plotting the number of rectified electrons as a function of the incident electric field exhibit different behaviours for the tips. However, after converting the incident electric field into the enhanced electric field, the curves exhibit almost the same behaviour (Fig. 3b), indicating that the tip geometry affects only the enhancement factor, and that the sharp tip can tightly focus the THz electric field.

The striking feature in Fig. 3b is the strong saturation of the tunnelling electrons observed above the enhanced electric field of  $6$  V nm<sup>-1</sup>, which was not predicted by the conventional Simmons model. A recent self-consistent calculation<sup>29</sup> predicted a new regime that deviates from the Simmons model at extremely high voltages, the so-called space-charge-limited regime, in which an additional space-charge potential plays an important role in limiting the current flow in the junction. In this calculation, the saturation of the tunnel currents occurred above  $6$  V nm<sup>-1</sup> with a workfunction of 4.08 eV; these values are in reasonably good agreement with our results. Note that this regime cannot be realized with a d.c. bias voltage or near-infrared pulses because the junction is easily damaged by Joule heating and high-energy photons, respectively<sup>20</sup>. Finally, we stress that an enhanced THz electric field of  $16$  V nm<sup>-1</sup> was achieved at the junction, which is two times higher than the strongest THz field previously reported in free space<sup>30</sup>. This spatially confined large single-cycle THz electric field can coherently drive the motion of as many as  $\sim 300,000$  electrons on the subpicosecond timescale.

In summary, we have demonstrated real-space coherent manipulation of electrons in a single tunnel junction. By utilizing CEP-controlled single-cycle THz electric fields, electron tunnelling can be induced either from the nanotip to the sample or vice versa. The extremely large field enhancement at the junction strongly modulates the potential barrier between the nanotip and the sample, leading to the strong saturation of rectified electrons in a space-charge-limited regime. We believe that this concept provides a new platform for the ultrafast coherent control of electrons, and may inspire a new route towards designing future nanoelectronics. Furthermore, our CEP-controlled THz-STM with an extremely high electric field is expected to be a powerful tool for exploring the ultrafast nonlinear control of matter<sup>22</sup> at the atomic scale.

## Methods

Methods and any associated references are available in the [Supplementary Information](#).

Received 19 April 2016; accepted 22 September 2016;  
published online 7 November 2016

## References

- Paulus, G. G. *et al.* Measurement of the phase of few-cycle laser pulses. *Phys. Rev. Lett.* **91**, 253004 (2003).
- Corkum, P. B. & Krausz, F. Attosecond science. *Nat. Phys.* **3**, 381–387 (2007).
- Schiffrin, A. *et al.* Optical-field-induced current in dielectrics. *Nature* **493**, 70–74 (2013).

4. Paasch-Colberg, T. *et al.* Solid-state light-phase detector. *Nat. Photon.* **8**, 214–218 (2014).
5. Luu, T. T. *et al.* Extreme ultraviolet high-harmonic spectroscopy of solids. *Nature* **521**, 498–502 (2015).
6. Hohenleutner, M. *et al.* Real-time observation of interfering crystal electrons in high-harmonic generation. *Nature* **523**, 572–575 (2015).
7. Krüger, M., Schenk, M. & Hommelhoff, P. Attosecond control of electrons emitted from a nanoscale metal tip. *Nature* **475**, 78–81 (2011).
8. Wimmer, L. *et al.* Terahertz control of nanotip photoemission. *Nat. Phys.* **10**, 432–436 (2014).
9. Piglowska, B. *et al.* Carrier-envelope phase effects on the strong-field photoemission of electrons from metallic nanostructures. *Nat. Photon.* **8**, 37–42 (2014).
10. Caulfield, H. J. & Dolev, S. Why future supercomputing requires optics. *Nat. Photon.* **4**, 261–263 (2010).
11. Krausz, F. & Stockman, M. I. Attosecond metrology: from electron capture to future signal processing. *Nat. Photon.* **8**, 205–213 (2014).
12. Ward, D. R., Hüser, F., Pauly, F., Cuevas, J. C. & Natelson, D. Optical rectification and field enhancement in a plasmonic nanogap. *Nat. Nanotech.* **5**, 732–736 (2010).
13. Vincent, R., Klyatskaya, S., Ruben, M., Wernsdorfer, W. & Balestro, F. Electronic read-out of a single nuclear spin using a molecular spin transistor. *Nature* **488**, 357–360 (2012).
14. Yoshida, K., Shibata, K. & Hirakawa, K. Terahertz field enhancement and photon-assisted tunneling in single-molecule transistors. *Phys. Rev. Lett.* **115**, 138302 (2015).
15. Sharma, A., Singh, V., Boughez, T. L. & Cola, B. A. A carbon nanotube optical rectenna. *Nat. Nanotech.* **10**, 1027–1032 (2015).
16. Savage, K. J. *et al.* Revealing the quantum regime in tunnelling plasmonics. *Nature* **491**, 574–577 (2012).
17. Tan, S. F. *et al.* Quantum plasmon resonances controlled by molecular tunnel junctions. *Science* **343**, 1496–1499 (2014).
18. Bahk, Y.-M. *et al.* Electromagnetic saturation of angstrom-sized quantum barriers at terahertz frequencies. *Phys. Rev. Lett.* **115**, 125501 (2015).
19. Cocker, T. L. *et al.* An ultrafast terahertz scanning tunnelling microscope. *Nat. Photon.* **7**, 620–625 (2013).
20. Grafström, S. Photoassisted scanning tunneling microscopy. *J. Appl. Phys.* **91**, 1717–1753 (2002).
21. Hirori, H., Doi, A., Blanchard, F. & Tanaka, K. Single-cycle terahertz pulses with amplitudes exceeding 1 MV/cm generated by optical rectification in LiNbO<sub>3</sub>. *Appl. Phys. Lett.* **98**, 091106 (2011).
22. Kampfrath, T., Tanaka, K. & Nelson, K. A. Resonant and nonresonant control over matter and light by intense terahertz transients. *Nat. Photon.* **7**, 680–690 (2013).
23. Yoshioka, K. *et al.* Terahertz-field-induced nonlinear electron delocalization in Au nanostructures. *Nano Lett.* **15**, 1036–1040 (2015).
24. Terada, Y., Yoshida, S., Takeuchi, O. & Shigekawa, H. Real-space imaging of transient carrier dynamics by nanoscale pump–probe microscopy. *Nat. Photon.* **4**, 869–874 (2010).
25. Yoshida, S. *et al.* Probing ultrafast spin dynamics with optical pump–probe scanning tunnelling microscopy. *Nat. Nanotech.* **9**, 588–593 (2014).
26. Feng, S. & Winful, H. G. Physical origin of the Gouy phase shift. *Opt. Lett.* **26**, 485–487 (2001).
27. Higuchi, T., Maisenbacher, L., Liehl, A., Dombi, P. & Hommelhoff, P. A nanoscale vacuum-tube diode triggered by few-cycle laser pulses. *Appl. Phys. Lett.* **106**, 051109 (2015).
28. Simmons, J. G. Generalized formula for the electric tunnel effect between similar electrodes separated by a thin insulating film. *J. Appl. Phys.* **34**, 1793–1803 (1963).
29. Zhang, P. Scaling for quantum tunneling current in nano- and subnano-scale plasmonic junctions. *Sci. Rep.* **5**, 9826 (2015).
30. Shalaby, M. & Hauri, C. P. Demonstration of a low-frequency three-dimensional terahertz bullet with extreme brightness. *Nat. Commun.* **6**, 5976 (2015).

### Acknowledgements

This work was supported in part by the Grants-in-Aid for Scientific Research (numbers 15H05734, 16H03820, 16H04001 and 16H06010) from the Japan Society for the Promotion of Science and the Ministry of Education, Culture, Sports, Science and Technology, and by the Strategic Information and Communications R&D Promotion Programme (SCOPE #145003103) of Japan Ministry of Internal Affairs and Communications.

### Author contributions

I.K., M.K., H.S. and J.T. conceived and coordinated this project. K.Y. designed and built the THz-STM set-up. K.Y. and Y.M. developed the intense THz generation system, and K.Y. and S.Y. constructed the operation program of the STM. K.Y. carried out the experiments and simulations with support from I.K., Y.M. and S.Y., and H.S., M.K. and J.T. contributed to the initial concept of the experiments. K.Y. and J.T. wrote the manuscript with contributions from all authors.

### Additional information

Supplementary information is available in the [online version of the paper](#). Reprints and permissions information is available online at [www.nature.com/reprints](#). Correspondence and requests for materials should be addressed to I.K., H.S. and J.T.

### Competing financial interests

The authors declare no competing financial interests.